

# Gene- and variant-specific efficacy of serum/glucocorticoid-regulated kinase 1 inhibition in long QT syndrome types 1 and 2

Federica Giannetti<sup>1†</sup>, Miriam Barbieri<sup>2†</sup>, Assad Shiti<sup>3†</sup>, Simona Casini<sup>4</sup>, Philip T. Sager<sup>5,6</sup>, Saumya Das<sup>5,7</sup>, Sabindra Pradhananga<sup>5</sup>, Dinesh Srinivasan<sup>5</sup>, Saranda Nimani<sup>2</sup>, Nicolò Alerni<sup>2</sup>, Julien Louradour<sup>2</sup>, Manuela Mura<sup>8</sup>, Massimiliano Gnechi<sup>8,9</sup>, Paul Brink<sup>10</sup>, Manfred Zehender<sup>11</sup>, Gideon Koren<sup>12</sup>, Antonio Zaza<sup>13</sup>, Lia Crotti<sup>1,14</sup>, Arthur A.M. Wilde<sup>4</sup>, Peter J. Schwartz<sup>1</sup>, Carol Ann Remme<sup>4</sup>, Lior Gepstein<sup>3,15‡</sup>, Luca Sala<sup>1,13‡</sup>, and Katja E. Odening<sup>2\*‡</sup>

<sup>1</sup>Istituto Auxologico Italiano IRCCS, Center for Cardiac Arrhythmias of Genetic Origin and Laboratory of Cardiovascular Genetics, Milan, Italy; <sup>2</sup>Translational Cardiology, Department of Cardiology and Department of Physiology, University Hospital Bern, University of Bern, Bülhplatz 5, 3012 Bern, Switzerland; <sup>3</sup>Rappaport Faculty of Medicine and Research Institute, Technion–Israel Institute of Technology, Haifa, Israel; <sup>4</sup>Amsterdam UMC Location AMC Department of Clinical and Experimental Cardiology, Heart Centre, Amsterdam, The Netherlands; <sup>5</sup>Thryv Therapeutics Inc., Montreal, Canada; <sup>6</sup>Cardiovascular Research Institute, Stanford University, Palo Alto, CA, USA; <sup>7</sup>Massachusetts General Hospital, Harvard Medical School, Boston, MA, USA; <sup>8</sup>Department of Cardiothoracic and Vascular Sciences–Translational Cardiology Center, Fondazione IRCCS Policlinico San Matteo, Pavia, Italy; <sup>9</sup>Department of Molecular Medicine, Unit of Cardiology, University of Pavia, Pavia, Italy; <sup>10</sup>Department of Medicine, University of Stellenbosch, Tygerberg, South Africa; <sup>11</sup>Department of Cardiology and Angiology I, University Heart Center Freiburg, University Medical Center Freiburg, Freiburg, Germany; <sup>12</sup>Cardiovascular Research Center, Brown University, Providence, RI, USA; <sup>13</sup>Department of Biotechnology and Biosciences, University of Milano-Bicocca, Milan, Italy; <sup>14</sup>Department of Medicine and Surgery, University of Milano-Bicocca, Milan, Italy; and <sup>15</sup>Cardiology Department, Rambam Health Care Campus, Haifa, Israel

Received 18 February 2023; accepted after revision 20 March 2023

## Aims

Current long QT syndrome (LQTS) therapy, largely based on beta-blockade, does not prevent arrhythmias in all patients; therefore, novel therapies are warranted. Pharmacological inhibition of the serum/glucocorticoid-regulated kinase 1 (SGK1-Inh) has been shown to shorten action potential duration (APD) in LQTS type 3. We aimed to investigate whether SGK1-Inh could similarly shorten APD in LQTS types 1 and 2.

## Methods and results

Human-induced pluripotent stem cell-derived cardiomyocytes (hiPSC-CMs) and hiPSC-cardiac cell sheets (CCS) were obtained from LQT1 and LQT2 patients; CMs were isolated from transgenic LQT1, LQT2, and wild-type (WT) rabbits. Serum/glucocorticoid-regulated kinase 1 inhibition effects (300 nM–10 µM) on field potential durations (FPD) were investigated in hiPSC-CMs with multielectrode arrays; optical mapping was performed in LQT2 CCS. Whole-cell and perforated patch clamp recordings were performed in isolated LQT1, LQT2, and WT rabbit CMs to investigate SGK1-Inh (3 µM) effects on APD. In all LQT2 models across different species (hiPSC-CMs, hiPSC-CCS, and rabbit CMs) and independent of the disease-causing variant (*KCNH2*-p.A561V/p.A614V/p.G628S/IVS9-28A/G), SGK1-Inh dose-dependently shortened FPD/APD at 0.3–10 µM (by 20–32%/25–30%/44–45%). Importantly, in LQT2 rabbit CMs, 3 µM SGK1-Inh normalized APD to its WT value. A significant FPD shortening was observed in *KCNQ1*-p.R594Q hiPSC-CMs at 1/3/10 µM (by 19/26/35%) and in *KCNQ1*-p.A341V hiPSC-CMs at 10 µM (by 29%). No SGK1-Inh-induced FPD/APD shortening effect was observed in LQT1 *KCNQ1*-p.A341V hiPSC-CMs or *KCNQ1*-p.Y315S rabbit CMs at 0.3–3 µM.

## Conclusion

A robust SGK1-Inh-induced APD shortening was observed across different LQT2 models, species, and genetic variants but less consistently in LQT1 models. This suggests a genotype- and variant-specific beneficial effect of this novel therapeutic approach in LQTS.

\* Corresponding author. Tel: +41 31 684 5402. E-mail address: katja.odening@unibe.ch

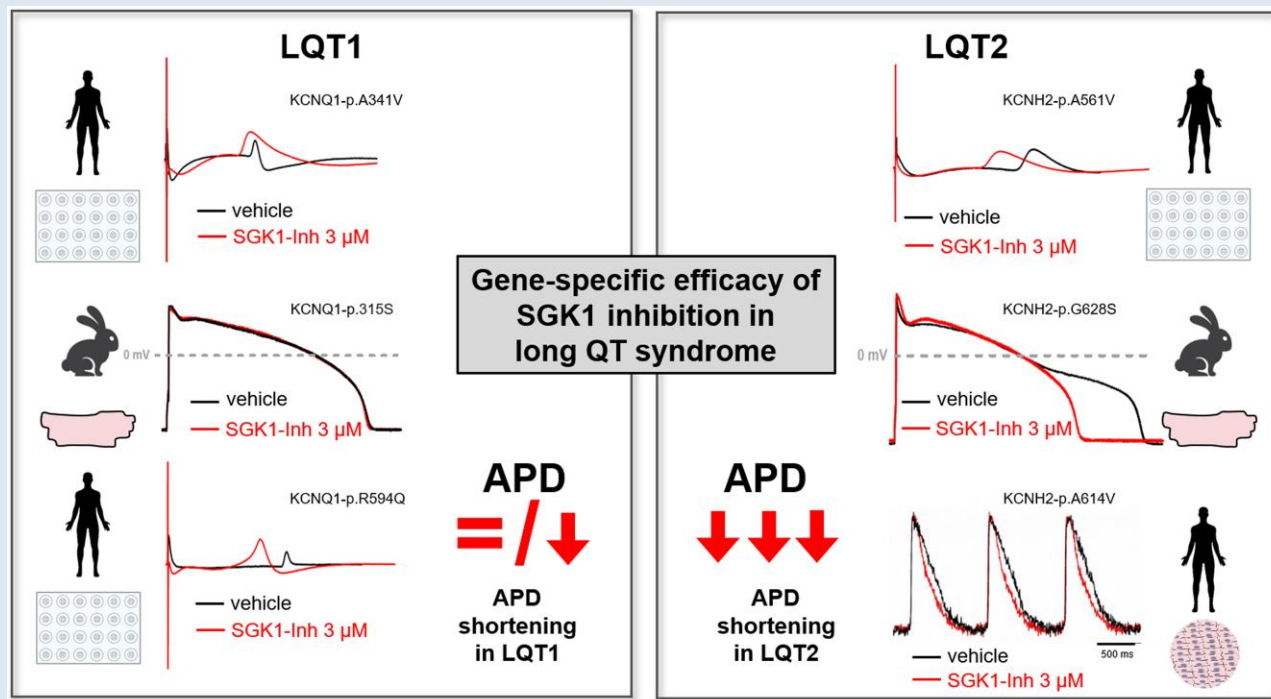
† These authors contributed equally as joint first authors.

‡ These authors contributed equally as joint last authors.

© The Author(s) 2023. Published by Oxford University Press on behalf of the European Society of Cardiology.

This is an Open Access article distributed under the terms of the Creative Commons Attribution-NonCommercial License (<https://creativecommons.org/licenses/by-nc/4.0/>), which permits non-commercial re-use, distribution, and reproduction in any medium, provided the original work is properly cited. For commercial re-use, please contact journals.permissions@oup.com

## Graphical Abstract



Illustrated are the effects of SGK1-Inh at 3  $\mu$ M in the different models/different variants.

## Keywords

LQTS • Genotype-specific therapy • Mechanism-based therapy • Cellular electrophysiology • hiPSC • Animal models

## What's new?

- Pharmacological inhibition of the serum/glucocorticoid-regulated kinase 1 has beneficial, shortening effects on repolarization in LQT2 human-induced pluripotent stem cell-derived cardiomyocytes (hiPSC-CMs), hiPSC-cardiac cell sheets, and rabbit CMs.
- Serum/glucocorticoid-regulated kinase 1 inhibition leads to a normalization of action potential duration to healthy levels in LQT2 in rabbit CMs.
- Serum/glucocorticoid-regulated kinase 1 inhibition has a variable impact on repolarization in LQT1 models, suggesting a gene- and variant-specific effect that warrants further exploration.
- Serum/glucocorticoid-regulated kinase 1 inhibition deserves further evaluation as a promising novel therapeutic approach in long QT syndrome.

## Introduction

On paper, the clinical management of long QT syndrome (LQTS) should be rather straightforward.<sup>1,2</sup> Beta-blockers are extremely effective, and whenever patients appear not fully protected, there are still three useful remaining tools: mexiletine (particularly in long QT types 2 and 3),<sup>3,4</sup> left cardiac sympathetic denervation (LCSD),<sup>5</sup> and implantable cardioverter defibrillator (ICD).<sup>6</sup> Unfortunately, however, the situation is complicated by the fact that a significant subset of patients does not sufficiently benefit from beta-blockers, poorly tolerates beta-blockers, or has a clear contraindication to the latter.<sup>7</sup> Indeed, in ~15% of the LQTS patients who experienced an aborted cardiac arrest while untreated, a further cardiac arrest occurred within 5 years after starting beta-blocker treatment, when no ICDs were implanted.<sup>8</sup> Fatal

arrhythmias may also occur as the first manifestation of the disease; individuals who survive typically receive an ICD,<sup>6</sup> which however negatively impacts quality of life and is often associated with severe complications such as inappropriate shocks, infections, lead rupture or dislocation, and vascular complications, particularly when implanted already at a young age. Clearly, a pharmacological alternative that normalizes cardiac repolarization would address an unmet need.

These considerations have recently led to the search for precision medicine approaches, which are essentially represented by gene- or variant-specific therapies largely based on drug studies in patient-specific human-induced pluripotent stem cell-derived cardiomyocytes (hiPSC-CMs)<sup>9–11</sup> or in LQTS animal models.<sup>12,13</sup> In addition to approaches targeting mutated channels, novel approaches include prevention of the pro-arrhythmic events secondary to action potential duration (APD) prolongation and resulting in the disruption of normal sodium ( $\text{Na}^+$ ) and calcium ( $\text{Ca}^{2+}$ ) homeostasis. Although alterations in intracellular  $\text{Na}^+$  and  $\text{Ca}^{2+}$  homeostasis have been linked to arrhythmogenesis in LQTS in general,<sup>14</sup> they have not been investigated as a potential therapeutic target in the different LQTS genotypes. Only in LQT3, in which the enhancement of the late sodium current (late  $I_{\text{Na}}$ ) arises as the mutation's primary consequence, the use of sodium channel blockers such as mexiletine demonstrated long-term benefit.<sup>15</sup> Novel therapies that tackle the pathophysiological mechanisms responsible for arrhythmogenesis are therefore clearly warranted—particularly for treating LQTS patients at the highest risk for potentially lethal ventricular arrhythmias or those in whom conventional approaches have failed.

The serum/glucocorticoid-regulated kinase 1 (SGK1) was recently identified as an important regulator of cardiac  $\text{Na}^+$  channels and other ionic transporters; its activation can lead to a marked alteration in the  $\text{Na}^+$  flux, an increased late  $I_{\text{Na}}$ , and a prolongation of APD if

pathologically up-regulated.<sup>16</sup> Consequently, the inhibition of SGK1 was demonstrated to shorten APD in LQT3 hiPSC-CMs.<sup>17</sup>

While late  $I_{Na}$  is not primarily affected by LQT1 and LQT2 mutations, several findings suggest that late  $I_{Na}$  may be enhanced also in genotypes associated with loss of function of  $K^+$  channels,<sup>18–20</sup> as recently demonstrated by the effectiveness of late  $I_{Na}$  blockers in animal models and patients with LQT2.<sup>19</sup> In addition, SGK1 has been shown to be activated by  $Ca^{2+}$ -calmodulin-dependent kinase II (CaMKII), suggesting that calcium homeostasis may play a role in the regulation of repolarization by SGK1.<sup>21</sup>

This considered, we aimed to comprehensively assess the effects of SGK1 inhibition in a set of *in vitro* and *ex vivo* models of the two most common LQTS genotypes—LQT1 and LQT2—which account for more than 85% of the genotyped LQTS cases.<sup>22</sup>

Here, we have harnessed the advantages of these complementary models<sup>13</sup> to (i) identify a potential range of concentrations of a potent SGK1 inhibitor (SGK1-Inh) to shorten the repolarization duration in LQT1 and LQT2 hiPSC-CMs, (ii) validate the most effective concentration in adult CMs from transgenic rabbits carrying additional LQT1 and LQT2 variants, and (iii) validate the concentrations in advanced human cardiac cell sheets (CCS) carrying a further LQT2 variant.

## Methods

### Ethical aspects

All animal experiments were performed in compliance with EU legislation (directive 2010/63/EU) and Swiss Animal Welfare Ordinance after approval by the Cantonal Veterinary Office and the Animal Welfare Officer (Kanton Bern, approval number BE132-20). Animal housing and handling were in accordance with good animal practice as defined by the Federation of European Laboratory Animal Science Associations (FELASA). Animal studies were reported in compliance with the ARRIVE guidelines.

All the patients involved in this study signed appropriate informed consent forms, and the study has been reviewed and received approval by the following Ethical Committees: Istituto Auxologico Italiano IRCCS in Milan; Fondazione IRCCS Policlinico San Matteo in Pavia; University of Stellenbosch, Tygerberg (South Africa); and Helsinki Committee of Rambam Medical Center.

### Compounds

The SGK1-Inh (provided by Thryv Therapeutics) was dissolved in DMSO (vehicle) to obtain a 10 mM stock solution and further diluted in RPMI-based medium or Tyrode solution to obtain the following concentrations: 10, 3, and 1  $\mu$ M and 300 nM. Of note, its selectivity for SGK1 inhibition had been examined in a biochemical assay, which assessed the kinase reactivity in a 50-kinase panel, and in a cell-based *in vitro* screening assay to determine its selectivity across a broad range of kinases, non-kinase enzymes, ion channels, G-protein-coupled receptors, and transporter proteins, all indicating that SGK1-Inh is highly selective. In all solutions, the final DMSO concentration was <0.1%, found to be devoid of effect on field potential durations (FPD) in multielectrode array (MEA) studies (see Figure 1) and in isolated rabbit CMs. For the other type of measurement, SGK1-Inh was compared to the DMSO-containing one (vehicle).

### Human-induced pluripotent stem cell lines

Human-induced pluripotent stem cell lines derived from two LQT1 and three LQT2 patients were used in this study. Clinical characteristics of the patients are provided in [Supplementary material online, Table S1](#). Three LQT1 hiPSC lines carry the heterozygous *KCNQ1*-p.A341V variant.<sup>23,24</sup> The other LQT1 line, previously published,<sup>25</sup> carries a heterozygous *KCNQ1*-p.R594Q variant. One LQT2 line carries a heterozygous trafficking-deficient variant in the hERG channel, namely the *KCNH2*-p.A561V variant.<sup>26–28</sup> This line was generated and kindly provided by Joseph C. Wu, MD, PhD, at the Stanford Cardiovascular Institute, funded by NHLBI BhiPSC-CVD 75N9202D00019. A second LQT2 line carries the branch point mutation *KCNH2*-IVS9-28A/G, which disrupts the acceptor

splice site definition of intron 9 and was associated with trafficking deficiency.<sup>29,30</sup> A third LQT2 line, used for optical mapping experiments, has been previously described<sup>18</sup> and is carrying the *KCNH2*-p.A614V variant—a heterozygous missense variant in the pore-forming region of the hERG channel resulting in both trafficking defect and altered channel inactivation properties.<sup>31</sup>

All pathogenic variants present in the different LQT1 and LQT2 hiPSC-CM (and rabbit) models are summarized in [Table 1](#).

### Human-induced pluripotent stem cell culture and cardiac differentiation

#### Human-induced pluripotent stem cell differentiation for multielectrode array experiments

Human-induced pluripotent stem cells were maintained in Essential8 Flex (ThermoFisher) on multiwell plates (Greiner) coated with recombinant human vitronectin (rhVTN, ThermoFisher) and replated two times a week at low density. Cardiac differentiation was achieved by the protocol previously published by Lian *et al.*<sup>46</sup> with minor modifications. Beating areas appeared after 7/9 days after inducing the cardiac differentiation. Cardiomyocytes were metabolically selected with glucose-deprived RPMI (Gibco) supplemented with B-27 (Gibco) and 4 mM (0.036% v/v) lactic acid (from 90%, Merck) from Days 9 to 12 after starting the differentiation, which has previously been shown to increase the purity of hiPSC-CM populations up to 99% as verified by the amount of cTnT+ cells by flow cytometry.<sup>47</sup> Human-induced pluripotent stem cell-derived cardiomyocytes were then cryopreserved directly after the metabolic starvation. Metabolically selected CMs were later thawed, and their yield was increased as published by Buikema *et al.*<sup>48</sup> Human-induced pluripotent stem cell-derived cardiomyocytes were cultured in RPMI 1640 (Euroclone) supplemented with B-27™ Supplement Minus Insulin (1X, Gibco) from Days 0 to 5. From Day 5 onwards, hiPSC-CMs were maintained in RPMI 1640 supplemented by B-27™ Supplement (1X, Gibco) and 1% KnockOut™ Serum Replacement (ThermoFisher), which was refreshed twice per week. After 2 weeks, hiPSC-CMs were dissociated into single cells with TrypLE Select 5X (ThermoFisher) and either cryopreserved or used for further experiments. Our previously published patch clamp data<sup>49</sup> demonstrate that, in these conditions, hiPSC-CMs exhibit a mature phenotype, and the relative amount of non-CMs as well as non-ventricular-like hiPSC-CMs is consistently very low.

#### Human-induced pluripotent stem cell differentiation for optical mapping experiments

Colonies of hiPSCs were cultured on 1:200 growth factor-reduced Matrigel using hESC mTeSR-1 cell culture medium. Cardiomyocyte differentiation was induced using the monolayer differentiation system as previously described.<sup>50,51</sup> To induce differentiation, 3–5 days after passaging or when the cells reached 80–90% confluence, the culture medium was switched to differentiation medium CDM3 [RPMI 1640, recombinant human serum albumin 500  $\mu$ g/mL, 213  $\mu$ g/mL L-ascorbic acid 2-phosphate, and 1% penicillin/streptomycin (100 U/mL and 100 g/mL, respectively) supplemented with 6  $\mu$ mol/L CHIR99021] for 2 days. On Day 2, the medium was replaced with CDM3 medium (without CHIR) supplemented with 2  $\mu$ mol/L WNT-C59 for additional 2 days. From Day 5 onwards, the cells were cultured with CDM3 medium, and the medium was refreshed every other day. On Days 8–10, spontaneous contraction could be identified in the differentiating monolayers. Routine flow cytometry analysis of the selected differentiations revealed highly enriched differentiated CMs (>80% cardiac troponin T positive), of which the vast majority (>85–90%) expressed the ventricular isoform MLC2v. These were then dissociated to single cells and reseeded as dense 20  $\mu$ L drops containing ~700 000 cells on Matrigel-coated 35 mm plastic dishes to yield homogenous hiPSC-CCS. Cells were left to attach to the plates for at least 6 h and then flooded with 2 mL RPMI/B-27. The medium was replenished twice a week.

### Multielectrode array measurements

After dissociation, hiPSC-CMs were plated on 24-well multiwell MEA plates coated with bovine fibronectin (40  $\mu$ g/mL, Merck) as previously described<sup>49</sup> and maintained in RPMI 1640 medium (see above); the medium was refreshed twice a week. Field potentials (FP) were recorded after 2 weeks.

Recordings were performed at 37°C with a multiwell MEA system (Multichannel Systems) for 2 min. The time points considered for the

analysis were: baseline (before the addition of either the DMSO vehicle or SGK1-Inh) and 3, 24, 48, and 168 h (7 days) after drug addition. The medium containing DMSO or SGK1-Inh was refreshed every 48 h.

The field potential duration, RR interval, and peak-to-peak amplitude (PtPAmpl) were obtained with Multiwell-Analyzer. Raw FPD values were corrected for the RR interval to obtain corrected FPD (cFPD) using Bazett's formula.<sup>52</sup> Corrected field potential durations were internally normalized by dividing each cFPD data point by its respective cFPD at baseline.

## Cardiomyocyte isolations

Adult New Zealand White wild-type (WT), transgenic LQT1 (KCNQ1-Y315S), and transgenic LQT2 (KCNH2-G628S) rabbits (Table 1) of both sexes (3–6 months, 13 rabbits)<sup>53</sup> were anaesthetized with an i.m. injection of ketamine S (12.5 mg/kg) and xylazine (3.75 mg/mL). Standard enzymatic digestion was used to isolate ventricular CMs.<sup>54</sup> After euthanasia with pentobarbital injection i.v., hearts were rapidly excised, cannulated by the aorta, and mounted on a Langendorff perfusion system, where they were washed with oxygenated, body-temperature Tyrode solution. Shortly afterwards, 0.1 mM EGTA-supplemented Tyrode was perfused for 5–7 min, followed by a 20–25 min step of collagenase digestion (Worthington type 1) in 80  $\mu\text{M}$   $\text{Ca}^{2+}$  Tyrode. The heart was then removed from the perfusion system, and the left ventricle was reduced into small pieces. The process was followed by sequential 5 min steps of collagenase digestion in 80  $\mu\text{M}$   $\text{Ca}^{2+}$  Tyrode buffered with 15 mM BSA. Cells were seeded in 0.2 mM  $\text{Ca}^{2+}$  at room temperature (RT) and used within 6 h.

## Patch clamp measurements

Action potential (AP) recordings in isolated left ventricular rabbit CMs were performed using an Axopatch 200B amplifier (Molecular Devices, USA). Voltage control, data acquisition, and data analysis were performed with pClamp 11.1/Clampfit (Axon Instruments). Borosilicate glass patch pipettes with a tip resistance of 3–3.6 M $\Omega$  were used. Action potentials were filtered at 2 kHz and digitized at 20 kHz. The SGK1-Inh was solubilized in DMSO as a stock solution of 10 mM; the final DMSO concentration was <0.001% in both SGK1-Inh solution and control bath solution. Patch clamp experiments were performed in single CMs after 2–6 h of incubation at RT with either DMSO or SGK1-Inh (3  $\mu\text{M}$ ).

## Action potential measurements in whole-cell configuration

In single isolated rabbit CMs, APs were measured at RT using normal Tyrode solution. Pipettes were filled with (in mM) 125 KCl, 5 NaCl, 1 MgCl<sub>2</sub> (H<sub>2</sub>O)6, 5 K<sub>2</sub>ATP, 10 HEPES, and 0.5 EGTA, pH 7.2 (KOH). Action potentials were elicited at 1 Hz by 3 ms,  $\approx 1.5\times$  threshold current pulses through the patch pipette. We analyzed resting membrane potential (RMP), AP amplitude (APA), maximal AP upstroke velocity ( $dV/dt_{\text{max}}$ ), and APD at 90% repolarization (APD<sub>90</sub>). Data from  $\approx 50$  consecutive APs were averaged, and due to the small liquid junction potential (5 mV), no correction was necessary.<sup>55</sup> In LQT2 CMs, repolarization was very unstable at 37°C with plenty of early afterdepolarizations, which made measurements of APD difficult; to address this problem, the experiments were performed at RT.

## Action potential measurements in perforated patch configuration

In a second set of experiments in isolated rabbit CMs, we switched to the perforated patch method (by using amphotericin-B 0.44 mM). Using this approach, which prevents intracellular dialysis by pipette content, repolarization was more stable, and we could run whole-cell measurements at 37°C. Action potentials were measured using a modified Tyrode solution containing (in mM) 140 NaCl, 5.4 KCl, 1.8 CaCl<sub>2</sub>, 1.0 MgCl<sub>2</sub>, 5.5 glucose, and 5 HEPES, pH 7.4 (NaOH). Pipettes were filled with (in mM) 125 K-gluconate, 20 KCl, 5 NaCl, 10 HEPES, and 0.44 amphotericin-B, pH 7.3 (KOH). Action potentials were elicited at 1 Hz by 3 ms,  $\approx 1.5\times$  threshold current pulses through the patch pipette. We analyzed RMP, APA,  $dV/dt_{\text{max}}$ , and APD<sub>90</sub>. Data from 10 consecutive APs were averaged, and potentials were corrected for the calculated liquid junction potential (15 mV).<sup>55</sup>

## Optical mapping

The optical mapping setup consisted of a high-speed EMCCD camera (Evolve® 512 Delta, Photometrics, 512  $\times$  512 pixels) mounted on a

fluorescent microscope (MVX10, Olympus) equipped with 0.25 NA 6.3X–63X (MVPLAPO 1X, Olympus). The default field of view achieved for illumination and imaging by setting the zoom body on 3.2X was 6.7 mm. The hiPSC-CCS were loaded with the voltage-sensitive dye FluoVolt diluted 1:1000 in RPMI/B-27 culture media at 37°C for 30 min. The tissues were excited using LEDs (X-Cite® TURBO, Excelitas Technologies) with a peak wavelength of 475, and emission was passed through 495 long-pass dichroic mirrors and filtered using a 525/50 band-pass filter (all from Chroma). Fluorescence was acquired at 4  $\times$  4 binning with a 3.84 ms sampling interval ( $\approx 260$  frames/second). An IDL-based custom-written software, courtesy of Prof. Bum-Rak Choi (Brown University), was used for the acquisition and analysis of optical mapping videos as previously described.<sup>56</sup> Analysis included the derivation of APD at 80% repolarization (APD<sub>80</sub>) maps along with the calculation of mean APD<sub>80</sub> for each specimen—the mean of APD<sub>80</sub> values obtained from each pixel within the CCS studied. The APD<sub>80</sub> was defined as the time interval between the local activation time (the point of the local maximum of the first derivative) and the time point of 80% repolarization. Human-induced pluripotent stem cell-derived cardiac cell sheets were incubated at 37°C with either the vehicle (DMSO, 0.01%) or SGK1-Inh (300 nM and 3  $\mu\text{M}$ ) for 4–6 h. Optical mapping experiments were carried out at a physiological temperature of 37°C while the tissues were electrically stimulated at a constant frequency of 1 Hz. For each hiPSC-CCS, the absolute mean APD<sub>80</sub> value was calculated as well as the percentage of change in mean APD<sub>80</sub> compared to the average of mean APD<sub>80</sub> values of DMSO-treated hiPSC-CCS in each independent experiment.

## Statistical analysis

All data were expressed and plotted as the mean  $\pm$  standard error of the mean (SEM). All statistical analyses were performed with GraphPad Prism, and statistical significance was defined as  $P < 0.05$ .

## Multielectrode array measurements

Data were collected from three independent differentiations for the LQT2-p.A561V and LQT1-p.R594Q hiPSC lines. Data for LQT1-p.A341V were obtained by pooling four independent differentiations of three KCNQ1-p.A341V hiPSC lines (see [Supplementary material online, Table S1](#)), generating a small cohort of carriers of the same variant. Sample sizes of the experiments are reported in the figure legends. Comparison with DMSO was calculated for the complete time course with two-way ANOVA followed by Dunnett's test to correct for multiple comparisons.

## Rabbit cardiomyocyte action potential measurements

Comparisons between the vehicle (DMSO)- and SGK1-Inh-treated cells were obtained by unpaired Student's *t*-test. The comparisons between the vehicle (DMSO) WT and LQT2 and SGK1-Inh-treated LQT2 cells were obtained with one-way repeated-measures ANOVA followed by Tukey's test for *post hoc* analysis.

## Optical mapping experiments

For each CCS, a mean APD<sub>80</sub> value was obtained, representing the mean of optical APD values measured for each pixel within the cell sheet. Comparison of the three treatment groups—vehicle (DMSO), 300 nM, and 3  $\mu\text{M}$ —was obtained with one-way repeated-measures ANOVA followed by Tukey's test for *post hoc* analysis.

# Results

## Differential effects of serum/glucocorticoid-regulated kinase 1 inhibition on field potential durations in LQT1 and LQT2 human-induced pluripotent stem cell-derived cardiomyocytes

We first investigated the effects of SGK1-Inh in LQT1 and LQT2 in hiPSC-CM-based models, allowing for concentration-finding experiments at different time points. The spontaneous beating rate was affected by SGK1-Inh with a dose-dependent shortening of RR

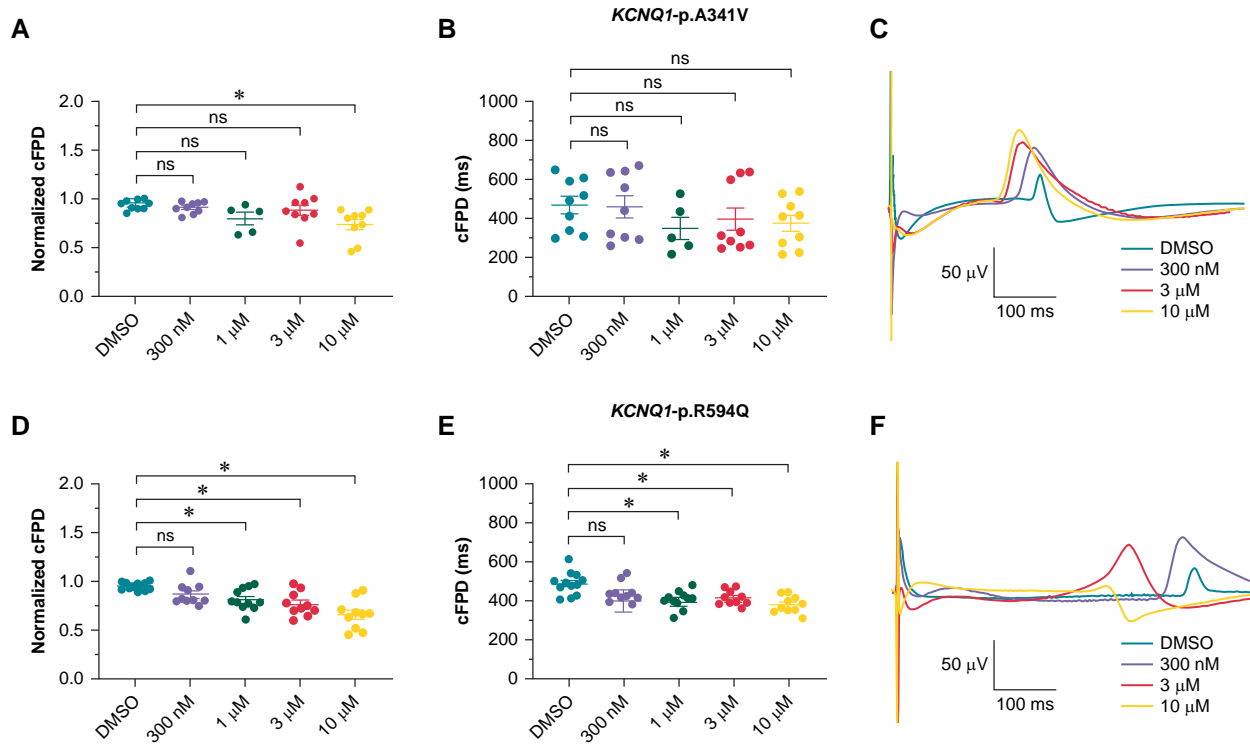


**Figure 1** Effect of SGK1-Inh on LQT1 hiPSC-CMs. (A) Dot plot comparing normalized cFPD after 3 h of incubation with DMSO or 0.3, 1, 3, or 10  $\mu\text{M}$  of SGK1-Inh in hiPSC-CMs carrying the *KCNQ1*-p.A341V variant.  $N = 9$ , at baseline from four independent differentiations of three *KCNQ1*-p.A341V hiPSC lines. (B) Dot plot comparing raw cFPD data after 3 h of incubation with DMSO or 0.3, 1, 3, or 10  $\mu\text{M}$  of SGK1-Inh in hiPSC-CMs carrying the *KCNQ1*-p.A341V variant. (C) Representative corrected FP traces after 3 h of incubation with DMSO or either 300 nM or 3  $\mu\text{M}$  of SGK1-Inh in hiPSC-CMs carrying the *KCNQ1*-p.A341V variant. (D) Dot plot comparing normalized cFPD after 3 h of incubation with DMSO or 0.3, 1, 3, or 10  $\mu\text{M}$  of SGK1-Inh in hiPSC-CMs with the *KCNQ1*-p.R594Q variant.  $N = 12$ , at baseline from three independent differentiations. (E) Dot plot comparing raw cFPD data after 3 h of incubation with DMSO or 0.3, 1, 3, or 10  $\mu\text{M}$  of SGK1-Inh in hiPSC-CMs with the *KCNQ1*-p.R594Q variant. (F) Representative corrected FP traces after 3 h of incubation with DMSO or either 300 nM or 3  $\mu\text{M}$  of SGK1-Inh in hiPSC-CMs with the *KCNQ1*-p.R594Q variant. \* $P < 0.05$  vs. DMSO. All samples are compared to the respective DMSO. Comparison with DMSO was calculated for the whole time course with two-way ANOVA followed by Dunnett's test to correct for multiple comparisons. cFPD, corrected field potential duration; FP, field potential; hiPSC-CMs, human-induced pluripotent stem cell-derived cardiomyocytes; ns, not significant; SGK1-Inh, serum/glucocorticoid-regulated kinase 1 inhibitor.

**Table 1** Summary of pathogenic variants investigated in the study

Gene	Pathogenic variants	Location of the variant within channel protein	Effects of the variant on channel function	Model system
<i>KCNQ1</i> (LQT1)	p.A341V	S6 segment	Normal protein trafficking. Mild dominant negative. Impaired PKA-dependent $I_{Ks}$ stimulation <sup>32–34</sup>	hiPSC-CMs
	p.R594Q	C-terminus	Trafficking deficiency <sup>35–38</sup>	hiPSC-CMs
	p.Y315S	Pore region	Dominant negative loss of function <sup>39</sup>	Transgenic rabbit
<i>KCNH2</i> (LQT2)	p.A561V	S5 segment	Trafficking deficiency. Dominant negative. Rescue not successful with E4031, low temperature, or thapsigargin <sup>27,40–42</sup>	hiPSC-CMs
	IVS9-28A/G	(Intronic)	Trafficking deficiency. Rescued by the proteasome inhibitor ALLN and lumacaftor <sup>30,42</sup>	hiPSC-CMs
	p.A614V	Pore region	Trafficking deficiency and altered inactivation. Not rescued by E4031, low temperature, or thapsigargin <sup>18,31,41,43,44</sup>	hiPSC-CCS
	p.G628S	Pore region	Dominant negative loss of function <sup>45</sup>	Transgenic rabbit

hiPSC-CCS, human-induced pluripotent stem cell-derived cardiac cell sheets; hiPSC-CMs, human-induced pluripotent stem cell-derived cardiomyocytes.

intervals, i.e. a fastening of the spontaneous beating rate, in all variants, requiring a rate correction of the FPD using Bazett's formula<sup>52</sup> (see [Supplementary material online, Figures S1 and S2](#)).

The SGK1-Inh had heterogeneous effects on the corrected cFPD of LQT1 hiPSC-CMs, with effects emerging mostly at high concentrations.

In LQT1 hiPSC-CMs carrying the *KCNQ1-p.A341V* variant, 1–10  $\mu\text{M}$  of SGK1-Inh numerically reduced the raw and normalized cFPD at 3 h, only reaching statistical significance at 10  $\mu\text{M}$  (by 26%) ([Figure 1A–C](#); see [Supplementary material online, Figure S1A–C](#)).

In LQT1 hiPSC-CMs carrying the *KCNQ1-p.R594Q* variant, 300 nM SGK1-Inh did not alter normalized cFPD. Conversely, 1, 3, and 10  $\mu\text{M}$  SGK1-Inh significantly decreased raw and normalized cFPD by 26–56% ([Figure 1D–F](#); see [Supplementary material online, Figure S1D–F](#)). The effect of SGK1-Inh decreased with time in LQT1 hiPSC-CMs and lasted for 48 h in *KCNQ1-p.A341V* and for 7 days in *KCNQ1-p.R594Q*, statistically significant only at the highest concentration tested (10  $\mu\text{M}$ ) (see [Supplementary material online, Figure S3](#)).

In LQT2 hiPSC-CMs, SGK1-Inh induced a prominent time- and concentration-dependent cFPD shortening, which lasted until 24 h (1  $\mu\text{M}$ ), 48 h (3  $\mu\text{M}$ ), or 7 days (10  $\mu\text{M}$ ) (see [Supplementary material online, Figure S4](#)).

In LQT2 hiPSC-CMs carrying the *KCNH2-p.A561V* variant, 300 nM SGK1-Inh did not affect cFPD. Normalized cFPD was decreased by 1, 3, and 10  $\mu\text{M}$  SGK1-Inh after 3 h (by 18–44%) ([Figure 2A–D](#)). Due to the very pronounced variation of raw cFPD in the different experiments, 300 nM and 1 and 3  $\mu\text{M}$  showed no significant effect on raw cFPD after 3 h ([Figure 2B](#); see [Supplementary material online, Figure S3A–C](#)). And 10  $\mu\text{M}$  SGK1-Inh significantly shortened also raw cFPD at all time points considered ([Figure 2A–C](#)).

In LQT2 hiPSC-CMs carrying the *KCNH2-IVS9-28A/G* splicing variant ([Figure 2D–F](#)), normalized cFPD was significantly shortened by all the concentrations from 300 nM to 10  $\mu\text{M}$  of SGK1-Inh at 3 h by 27–40%. Similarly, raw cFPD data showed a significant reduction after 3 h treatment at all concentrations from 300 nM to 10  $\mu\text{M}$  ([Figure 2E and F](#); see [Supplementary material online, Figure S3D–F](#)).

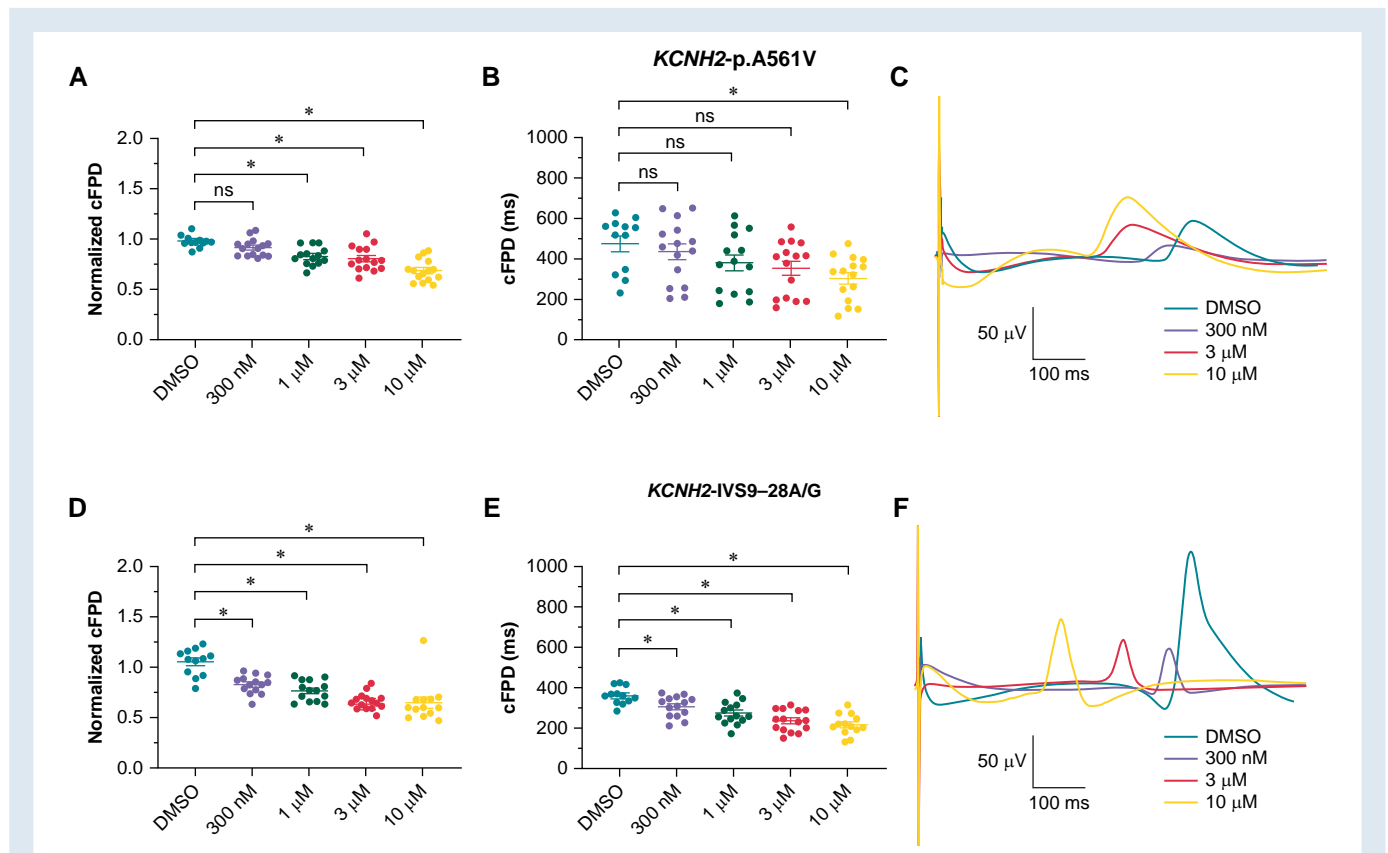


**Figure 2** Effect of SGK1-Inh on LQT2 hiPSC-CMs. (A) Dot plot comparing normalized cFPD after 3 h of incubation with DMSO or 0.3, 1, 3, or 10  $\mu\text{M}$  of SGK1-Inh in hiPSC-CMs with the *KCNH2-p.A561V* variant.  $N \geq 12$ , from three independent differentiations. (B) Dot plot comparing raw cFPD data after 3 h of incubation with DMSO or 0.3, 1, 3, or 10  $\mu\text{M}$  of SGK1-Inh in hiPSC-CMs with the *KCNH2-p.A561V* variant. (C) Representative corrected FP traces after 3 h of incubation with DMSO or either 300 nM or 3  $\mu\text{M}$  of SGK1-Inh in hiPSC-CMs with the *KCNH2-p.A561V* variant. (D) Dot plot comparing normalized cFPD after 3 h of incubation with DMSO or 0.3, 1, 3, or 10  $\mu\text{M}$  of SGK1-Inh in hiPSC-CMs with the *KCNH2-IVS9-28A/G* variant.  $N \geq 12$  at baseline from three independent differentiations. (E) Dot plot comparing raw cFPD data after 3 h of incubation with DMSO or 0.3, 1, 3, or 10  $\mu\text{M}$  of SGK1-Inh in hiPSC-CMs with the *KCNH2-IVS9-28A/G* variant.  $N \geq 12$  at baseline from three independent differentiations. (F) Representative corrected FP traces after 3 h of incubation with DMSO or either 300 nM or 3  $\mu\text{M}$  of SGK1-Inh in hiPSC-CMs with the *KCNH2-IVS9-28A/G* variant. \* $P < 0.05$  vs. DMSO. All samples are compared to the respective DMSO. Comparison with DMSO was calculated for the whole time course with two-way ANOVA followed by Dunnett's test to correct for multiple comparisons. cFPD, corrected field potential duration; FP, field potential; hiPSC-CMs, human-induced pluripotent stem cell-derived cardiomyocytes; ns, not significant; SGK1-Inh, serum/glucocorticoid-regulated kinase 1 inhibitor.

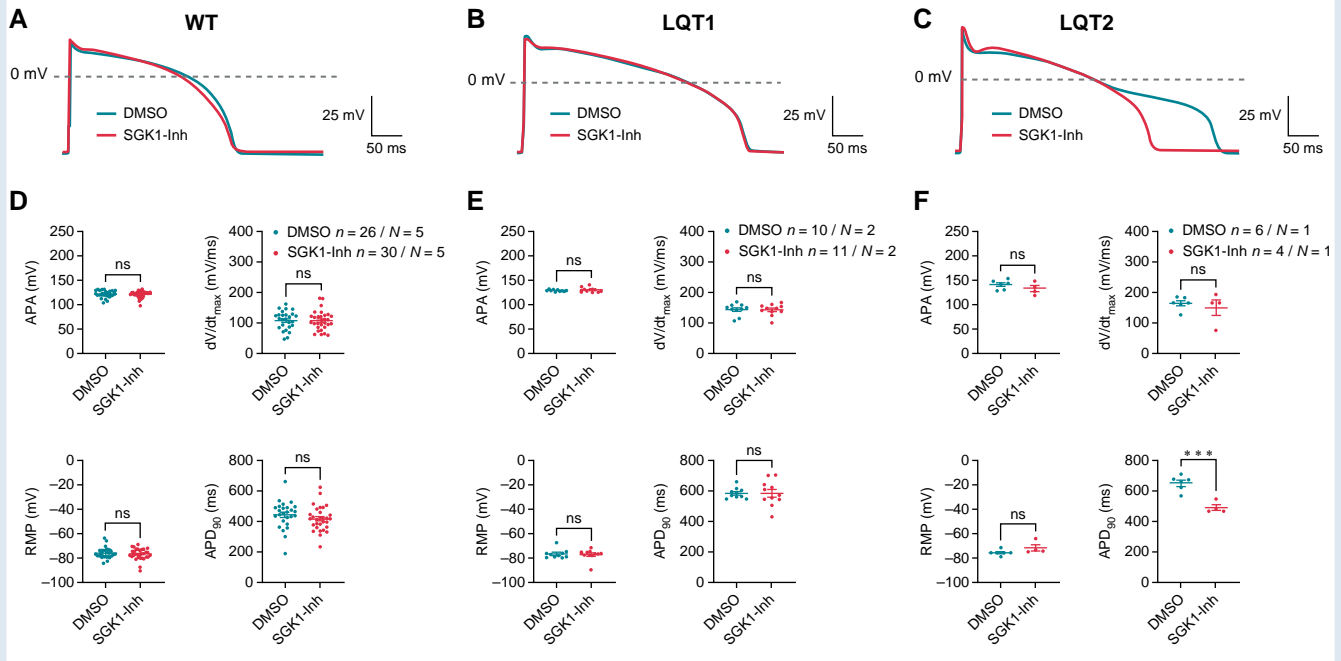


**Figure 3** Effects of SGK1-Inh on AP characteristics in isolated ventricular rabbit CMs in whole-cell configuration at RT. (A–C) Representative AP traces triggered at 1 Hz in WT (A), LQT1 (B), and LQT2 (C) isolated rabbit CMs treated with DMSO (vehicle) and after 2–6 h of incubation at RT with SGK1-Inh (3  $\mu$ M). (D–F) Average values for APA, RMP,  $dV/dt_{max}$ , and  $APD_{90}$  with DMSO and after SGK1-Inh incubation (3  $\mu$ M) in WT (five rabbits), LQT1 (two rabbits), and LQT2 (one rabbit). Results are expressed as mean  $\pm$  SEM, and every dot represents an individual value derived from one CM ( $n$ ).  $N$ , number of animals. \*\*\* $P < 0.001$ . Unpaired Student's  $t$ -test. AP, action potential; APA, AP amplitude;  $APD_{90}$ , action potential duration at 90% repolarization; CMs, cardiomyocytes;  $dV/dt_{max}$ , maximal AP upstroke velocity; ns, not significant; RMP, resting membrane potential; RT, room temperature; SEM, standard error of the mean; SGK1-Inh, serum/glucocorticoid-regulated kinase 1 inhibitor; WT, wild type.

## Differential effects of serum/glucocorticoid-regulated kinase 1 inhibition on action potential duration in LQT1/LQT2 rabbit cardiomyocytes

As a second step, we tested the effect of SGK1-Inh on AP parameters in isolated left ventricular LQT1 (*KCNQ1-Y315S*) and LQT2 (*KCNH2-G628S*) rabbit CMs to investigate whether we could observe similar genotype-specific effects. As we saw consistent significant APD shortening effects of SGK1-Inh in both LQT2 hiPSC lines starting from 300 nM/3  $\mu$ M as well as in one LQT1 hiPSC-CM line at 3  $\mu$ M, we proceeded with using a similar concentration of 3  $\mu$ M for the rabbit CM experiments.

We initially performed patch clamp experiments using the whole-cell configuration (Figure 3). Of note, as we observed plenty of early after-depolarizations using this method in LQT2 CMs at 37°C, we had to perform these experiments at RT.

In healthy WT and LQT1 CMs treated with SGK1-Inh, no effect was observed on  $APD_{90}$  compared to DMSO vehicle cells. Similarly, none of the other AP characteristics investigated—such as APA, RMP, and  $dV/dt_{max}$ —were altered (Figure 3A, B, D, and E).

In contrast, SGK1-Inh incubation (3  $\mu$ M) led to a significant shortening of  $APD_{90}$  in LQT2 CMs (Figure 3C and F). Similar to that in the hiPSC-CMs, this shortening was by 26%; and—importantly—led to a normalization of APD in the SGK1-Inh-treated LQT2 CMs to the WT level (Figure 5A and C).

In a second set of experiments, we performed similar AP experiments using the perforated patch clamp technique (Figure 4). This configuration is known to prevent changes in membrane currents due to

diffusional exchange between the cytoplasm and the content of the pipette ('washout')<sup>57</sup> resulting in more stable conditions also in LQT2 CMs, allowing us to perform these experiments at 37°C. Thus, we could also test the impact of the compound on cardiac AP in a more physiological condition—and investigate a potential impact of the temperature on the drug's efficacy.

Similar to that at RT, in WT CMs, no SGK1-Inh effect on  $APD_{90}$  or any of the other AP parameters studied (e.g. APA, RMP, and  $dV/dt_{max}$ ) was observed compared to baseline and DMSO vehicle cells (Figure 4A and C).

In LQT2 CMs, in contrast, also at 37°C, SGK1-Inh had a significant  $APD_{90}$  shortening effect of 21% (Figure 4B and D). And importantly, here again, the treatment with SGK1-Inh led to a normalization of the  $APD_{90}$  in LQT2 CMs to the WT level (Figure 5B and C).

## Effects of serum/glucocorticoid-regulated kinase 1 inhibition on repolarization in LQT2 human-induced pluripotent stem cell-derived cardiac cell sheets

Finally, we assessed the effect of SGK1-Inh on repolarization properties in a two-dimensional (2D) LQT2 cardiac tissue model.<sup>51,56</sup> Specifically, we utilized the previously established *KCNH2-p.A614V-LQT2* hiPSC-CM cell line<sup>18</sup> for generating a 5 mm-diameter CCS consisting of nearly 700 000 cells each. These specimens were incubated for 4–6 h at 37°C with either 300 nM or 3  $\mu$ M SGK1-Inh or DMSO (0.01%) as a vehicle control and were then studied under an optical mapping system.

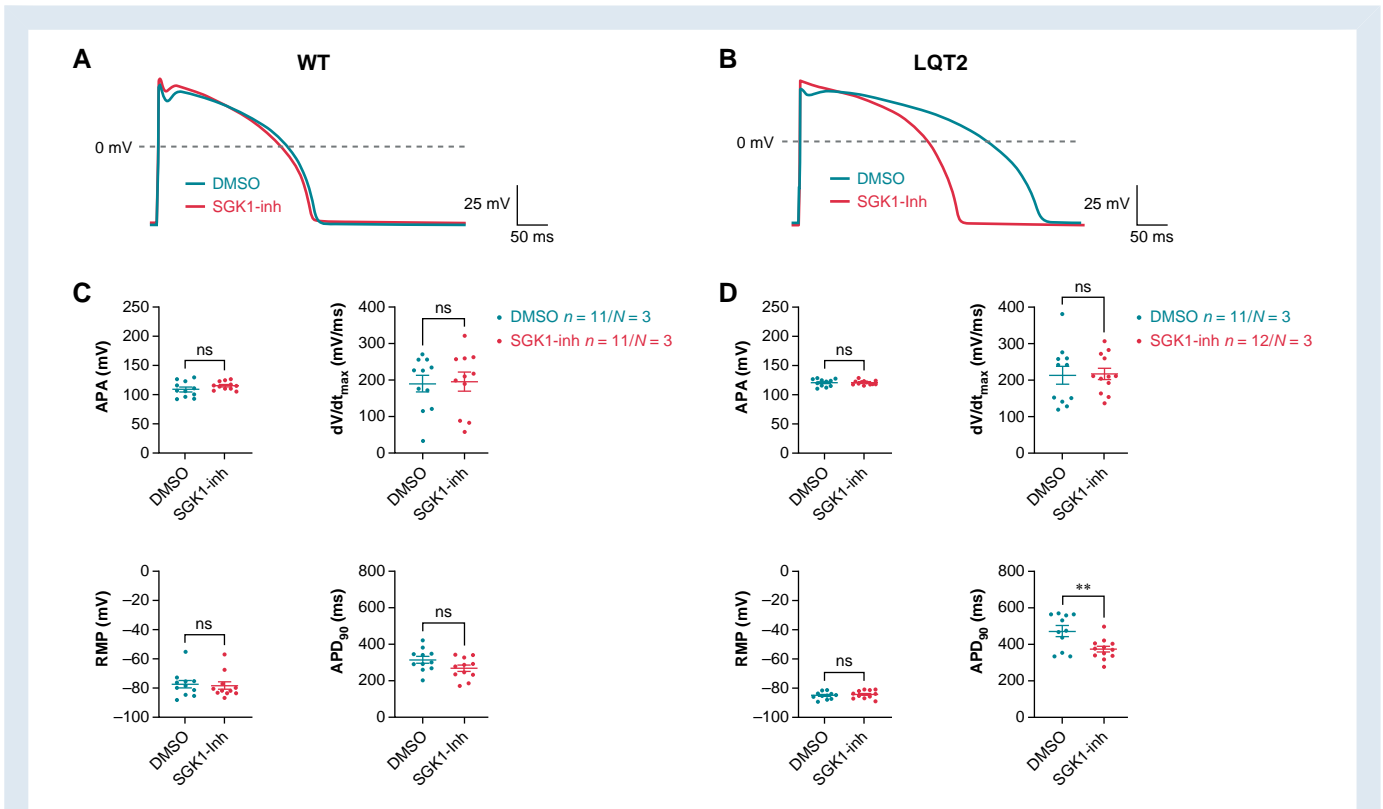


**Figure 4** Effects of SGK1-Inh on AP characteristics in isolated ventricular rabbit CMs in perforated patch configuration at 37°C. (A and B) Representative AP traces elicited at 1 Hz WT (A) and LQT2 (B) isolated rabbit ventricular CMs treated with DMSO (vehicle) and after 2–6 h of incubation at 37°C with SGK1-Inh (3  $\mu$ M). (C and D) Average values for APA, RMP, dV/dt<sub>max</sub>, and APD<sub>90</sub> with DMSO and after SGK1-Inh incubation (3  $\mu$ M) in WT (three rabbits) and LQT2 (three rabbits). Results are expressed as mean  $\pm$  SEM, and every dot represents an individual value derived from one CM (*n*). *N*, number of animals. \*\**P* < 0.005. Unpaired Student's *t*-test. AP, action potential; APA, AP amplitude; APD<sub>90</sub>, action potential duration at 90% repolarization; CMs, cardiomyocytes; dV/dt<sub>max</sub>, maximal AP upstroke velocity; ns, not significant; RMP, resting membrane potential; SEM, standard error of the mean; SGK1-Inh, serum/glucocorticoid-regulated kinase 1 inhibitor; WT, wild type.

LQT2 hiPSC-CCS pre-treated with 3  $\mu$ M SGK1-Inh had a significantly shorter mean APD<sub>90</sub> (267.6  $\pm$  26.7 ms vs. 369  $\pm$  27.8 ms, 1 Hz pacing, *P* < 0.05, Figure 6A–C) when compared to DMSO vehicle-treated tissues. The APD shortening effect was  $\sim$ 30% (Figure 6D, *P* < 0.0001), similar to the effect observed in MEA studies of hiPSC-CMs and patch clamp studies in rabbit CMs harbouring different LQT2 pathogenic variants. Treatment of LQT2 hiPSC-CCS with a lower concentration of 300 nM SGK1-Inh failed to shorten APD<sub>90</sub> in a statistically significant manner [326.1  $\pm$  23.1 vs. 369  $\pm$  27.8 ms, *P* = non-significant (ns)]. However, when evaluating the % APD shortening, a significant 12% shortening of APD<sub>90</sub> was observed (Figure 6D, *P* < 0.05), indicating a dose-dependent effect of SGK1-Inh on APD shortening.

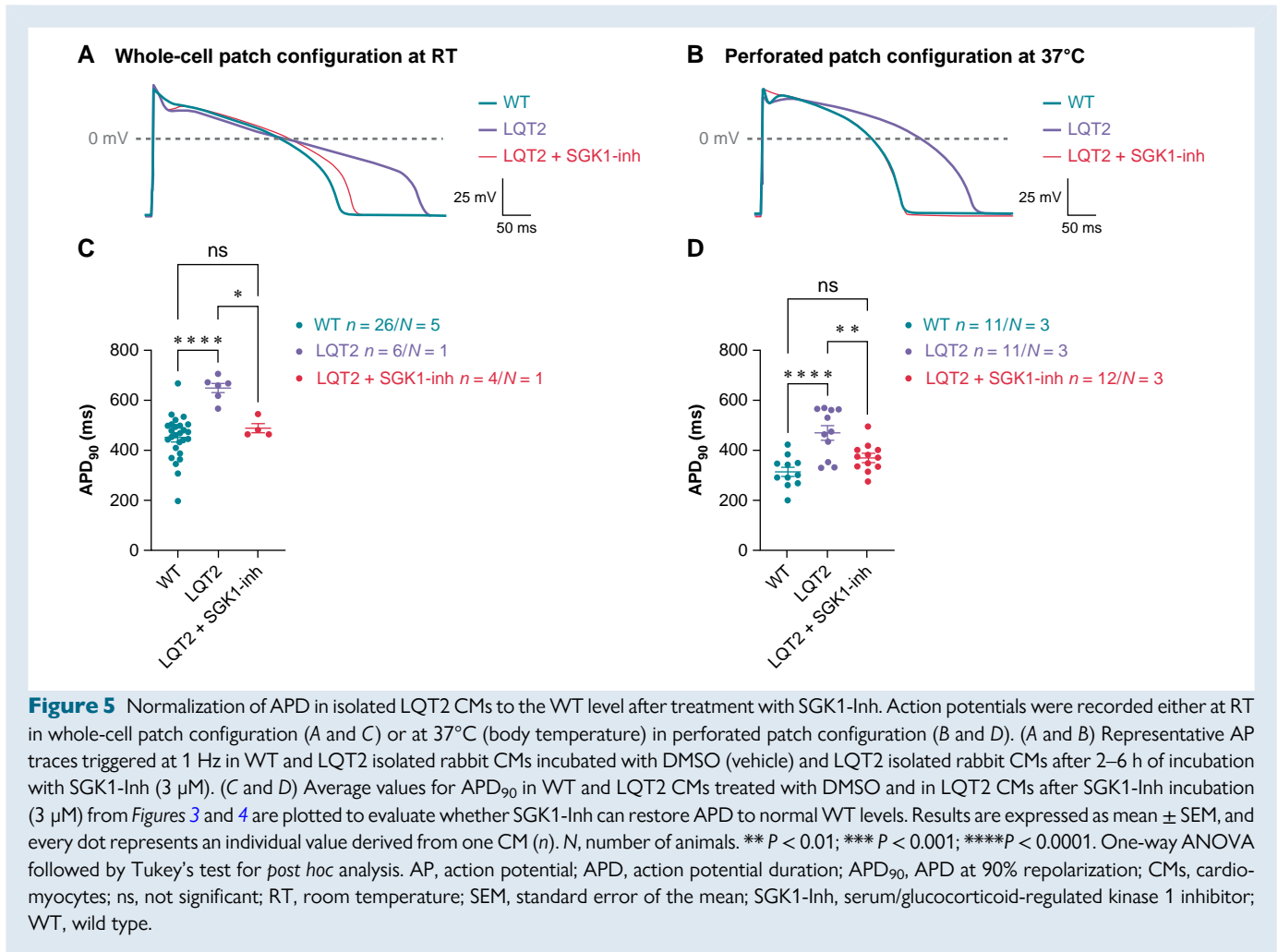
## Discussion

We investigated a novel therapeutic strategy for LQTS in a unique approach employing both hiPSC-CM and rabbit models of LQT1 and LQT2. Previously, inhibition of SGK1 was found to shorten APD in LQTS type 3 hiPSC-CMs.<sup>17</sup> We here demonstrate that pharmacological SGK1 inhibition also has a marked beneficial effect in LQT2, inducing a consistent shortening of the APD by 20–30% in different model systems (hiPSC-CMs, isolated CMs, and hiPSC-derived 2D tissues), in different species (human and rabbit), and with different *KCNH2* pathogenic variants (dominant negative pore mutations and trafficking defects). The fact that similar concentrations of the SGK1-Inh, e.g.

3  $\mu$ M, caused a similar degree of APD shortening in the different model systems and species further underlines that this effect may be generalizable. Importantly, when comparing the APD in LQT2 rabbit CMs treated with 3  $\mu$ M of SGK1-Inh to the APD in healthy WT CMs, it became evident that SGK1 inhibition can normalize the APD completely, strongly suggesting that it is a promising novel treatment approach also in LQT2. However, further future investigations on potential anti-arrhythmic effects on the tissue, whole-heart, and *in vivo* levels are of course warranted to investigate its full translational potential.

In addition to LQT3, secondary intracellular pro-arrhythmic changes leading to abnormal Na<sup>+</sup> and Ca<sup>2+</sup> homeostasis have also been demonstrated in LQT2.<sup>58</sup> Moreover, late *I*<sub>Na</sub> was also identified as a potential target for novel anti-arrhythmic agents in LQT2, as it was demonstrated that the late *I*<sub>Na</sub> inhibitor GS967 could suppress polymorphic VT formation in transgenic LQT2 hearts by accelerating Na<sup>+</sup>/Ca<sup>2+</sup> exchanger (*I*<sub>NCX</sub>)-mediated Ca<sup>2+</sup> efflux, shortening Ca<sup>2+</sup> transient duration, and reducing Ca<sup>2+</sup>-mediated EADs.<sup>20</sup> Similarly, Na<sup>+</sup>-channel blockers such as mexiletine were shown to be able to shorten APD and reduce pro-arrhythmic APD heterogeneity in drug-induced canine wedge preparations<sup>59</sup> and to shorten QTc in human LQT2 patients,<sup>19</sup> while ranolazine was shown to shorten APD and prevent cellular indices of arrhythmogenicity in a LQT2 hiPSC-CM model.<sup>18</sup> Serum/glucocorticoid-regulated kinase 1 is activated during pathological conditions such as haemodynamic stress and heart failure,<sup>60</sup> and mice with cardiac-specific deletion of SGK1 are protected from the development of heart failure, cardiac dilation, and fibrosis after pressure overload.<sup>16</sup>



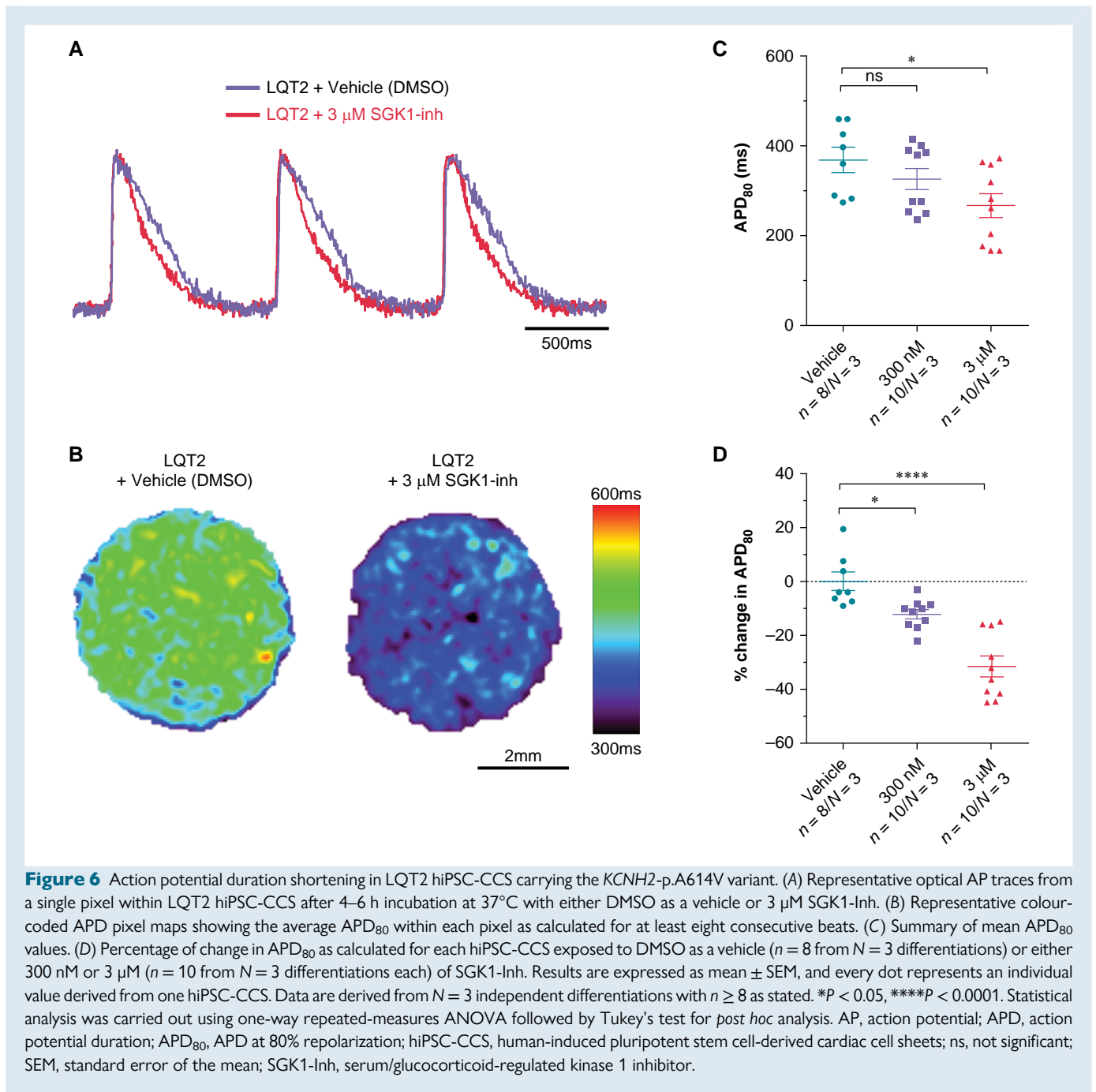


Conversely, mice with constitutively active SGK1 showed increased arrhythmia susceptibility and AP prolongation.<sup>16</sup> The latter could be prevented by the late  $I_{Na}$  inhibitor ranolazine, and SGK1 activation was found to be associated with increased late  $I_{Na}$ , potentially through its direct binding to  $Na_v1.5$  and consequent impact on channel gating.<sup>17</sup> Hence, a pathologically up-regulated SGK1 can lead to a marked alteration in the  $Na^+$  flux, an increased late  $I_{Na}$ , and an APD prolongation.<sup>16</sup> The SGK1-mediated increase of late  $I_{Na}$  may additionally lead to an increase of cytosolic calcium, which activates the CaMKII and thus further increases SGK1 activity and late  $I_{Na}$ .<sup>21</sup> This deleterious feed-forward loop might be interrupted by a pathway-targeted approach by SGK1-Inh. Moreover, other consequences of SGK1 inhibition may contribute to the observed effects on repolarization, which requires future investigation. In line with our observations, a recent publication demonstrated a successful APD shortening by SGK1 inhibition also in drug-induced LQTS due to  $I_{Kr}$  blockade,<sup>61</sup> which might be linked to the observation that  $I_{Kr}$  blockade may augment late  $I_{Na}$  via PI3K-dependent mechanisms.<sup>62</sup>

In contrast to our findings in LQTS2, the effect of SGK1 inhibition in LQTS1 seems to be more complex with variable effects in three different  $KCNQ1$  variants, suggesting genotype-specific differences—similar to those observed for ECG-based risk descriptors in LQTS patients.<sup>63</sup> Interestingly, while we observed no APD/FPD shortening in LQTS1 in two  $KCNQ1$  variants at 0.3–3 μM, a significant shortening was observed in the  $KCNQ1$ -p.R594Q variant at 1–10 μM and in the  $KCNQ1$ -p.A341V LQTS1 variant only at the highest 10 μM concentration. Importantly,

these differences cannot be attributed to potential species differences, as a reduced APD/FPD shortening efficacy was observed in different  $KCNQ1$  variants in both rabbit CMs and hiPSC-CMs. While it is known that differences in the extent of repolarization prolongation/baseline APD can explain differences in the extent of APD shortening effects of a given drug in general with more pronounced APD shortening effects in conditions with longer baseline APD,<sup>64</sup> this does not explain the differences among  $KCNQ1$  variants as the LQTS1 hiPSC-CMs with less obvious SGK1-Inh effects have a longer baseline cFPD—and interestingly, we do see similar FPD shortening effects in the different LQTS2  $KCNH2$  variants despite the baseline differences in their FPD. Moreover, variability in FPD among the different hiPSC-CM differentiations at baseline exhibited comparable levels between the  $KCNQ1$ -p.A341V variant, on which the effects of SGK1-Inh were reduced, and the LQTS2 variants, which conversely showed robust effects when treated with the SGK1-Inh, indicating that FPD dispersion cannot account for potential differences in the observed FPD shortening effects. Thus, while we cannot definitively exclude that a modest effect on the raw cFPD of the  $KCNQ1$ -p.A341V was masked by variability in the FPD, the differences in normalized cFPD data are more likely due to a potential variant-specific effect in LQTS1, possibly due to differential regulation of SGK1 in LQTS1 vs. LQTS2 cells.

Another potential explanation for variable APD shortening effects in LQTS1 may be provided by ancillary  $I_{Kr}$  blockade by SGK1-Inh, which may counteract late  $I_{Na}$ -blocking effects in LQTS1. In LQTS1,  $I_{Kr}$  prevails in supporting repolarization due to the genetic reduction of  $I_{Ks}$ , thus



making even partial  $I_{K_r}$  inhibition more likely to prolong it.<sup>65</sup> This might outbalance late  $I_{Na}$  reduction in setting the effects of SGK1-Inh on repolarization; nonetheless, the beneficial effects of reducing  $Na^+$  influx would be retained. In LQT2 models with already-marked  $I_{K_r}$  reduction or even absent  $I_{K_r}$  in contrast, this  $I_{K_r}$ -blocking property might not have such a big additional effect on cardiac repolarization. However, the lack of an effect of SGK1 inhibition on APD in the wild-type rabbit may argue against this hypothesis. Another explanation for the variant-specific differences in the efficacy of SGK1-Inh in LQT1 might lie in the fact that SGK1 may interact with *KCNQ1* channels directly via its N-terminal juxta-membranous domain, as demonstrated by Seeböhm et al.<sup>66</sup> The point mutations of the pathogenic *KCNQ1* variants included in our study, however, are all located outside the N-terminus of

*KCNQ1*, so either they have no direct effect on SGK1 binding or they may provide conformational or long-distance interactions with the SGK1 binding site on *KCNQ1*. Molecular modelling would be required to further elucidate this aspect.

A more potent SGK1-Inh might also have a more consistent benefit in LQT1, as recently reported with a different SGK1-Inh in LQT1 and LQT2 hiPSC-CMs, demonstrating a significant APD shortening in both genotypes.<sup>67</sup> In that study, however, only one single pathogenic *KCNQ1* variant was investigated, so it remains unclear whether the efficacy is due to different molecules or due to intrinsic properties of the *KCNQ1* variant used in this study.

Overall, the exact mechanism by which the SGK1-Inh exerts consistent APD shortening effects in LQT2—and why this is not consistently

observed in the three studied LQT1 variants—awaits further exploration.

## Limitations

No isogenic controls were used as the focus of the hiPSC-CM investigations was screening experiments to assess whether SGK1 inhibition had an effect in various *KCNQ1* and *KCNH2* variants and at which concentrations. This provided us with a valuable concentration range to proceed further with experiments in rabbits. Moreover, it has been previously shown that the beneficial effects of SGK1-Inh were restricted to LQT3 hiPSC-CMs, while no effects were observed in WT hiPSC-CM controls.<sup>17</sup>

The exact mechanism by which SGK1-Inh shortens APD/FPD in LQTS and—particularly—the causes for variant-specific sensitivities in LQT1 have not yet been identified. Here, detailed mechanistic studies are clearly warranted. Our combined use of multiple different cellular, cell sheet, and animal models will allow us to conduct further future studies on potential anti-arrhythmic effects also on the tissue and whole-heart levels, and potentially *in vivo*, which are mandatory prerequisites before translating these findings into first-in-men clinical pilot studies.

## Conclusions

In conclusion, this study demonstrates that the beneficial effect of SGK1 inhibition is not limited to LQTS type 3, which is primarily based on  $I_{NaL}$  enhancement, but it extends to LQTS subtypes associated with pathogenic variants in  $K^+$  channel genes. We observed a robust APD shortening effect in a variety of different models and species, independent of the underlying *KCNH2* mutation in LQTS type 2, resulting even in a complete APD normalization in LQT2 rabbit models—but a variable APD shortening in three different LQTS type 1 variants, suggesting a gene- and variant-specific efficacy of SGK1 inhibition in LQTS. This observation further underlines the importance of genetic testing in LQTS to guide future specific therapies.<sup>68</sup> Serum/glucocorticoid-regulated kinase 1 inhibition may be a promising novel treatment option in LQT2 and LQT3, in which beta-blockade provides a lower anti-arrhythmic efficacy compared to LQT1,<sup>69</sup> thereby filling the current gap in available treatment options. The mechanisms underlying the observed variable SGK1 inhibition in LQT1 need further exploration. Additionally, further investigations on potential anti-arrhythmic effects in tissue, whole-heart, and *in vivo* levels are warranted to investigate its full translational potential and potential unwanted side effects.

## Supplementary material

Supplementary material is available at *Europace* online.

## Acknowledgements

P.J.S., A.A.M.W., and L.C. are members of the European Reference Network for rare, low prevalence, and complex diseases of the heart: ERN GUARD-Heart (ERN GUARDHEART; <http://guardheart.ern-net.eu>).

## Funding

European Joint Research Program on Rare Diseases (EJP-RD) grant 'Silence-LQTS' (SNF No. 31ER30\_194836) to A.A.M.W., C.A.R., K.E.O., L.C., and L.G. Italian Ministry of Health Ricerca Corrente grant 'Registry of Cardiac Channelopathies' to L.C. and P.J.S. Italian Ministry of Health Ricerca Corrente grant 'Induced pluripotent stem cells to model rare cardiovascular diseases and to discover novel personalized therapies' to M.G. Fondazione CARIPLO 'Biomedical Research Conducted by Young Researchers' grant (No. 2019-1691) to L.S. Leducq Foundation for Cardiovascular Research (18CVD05) 'Towards Precision Medicine with

Human iPSCs for Cardiac Channelopathies' to P.J.S. European Research Council (ERC-2017-COG-773181-iPS-ChOp-AF) to L.G.

**Conflict of interest:** None declared.

## Data availability

All data are made available upon reasonable request.

## References

- Schwartz PJ, Ackerman MJ. The long QT syndrome: a transatlantic clinical approach to diagnosis and therapy. *Eur Heart J* 2013;**34**:3109–16.
- Wilde AAM, Amin AS, Postema PG. Diagnosis, management and therapeutic strategies for congenital long QT syndrome. *Heart* 2022;**108**:332–8.
- Schwartz PJ, Priori SG, Locati EH, Napolitano C, Cantù F, Towbin JA *et al*. Long QT syndrome patients with mutations of the *SCN5A* and *HERG* genes have differential responses to  $Na^+$  channel blockade and to increases in heart rate. Implications for gene-specific therapy. *Circulation* 1995;**92**:3381–6.
- Wilde AAM, Remme CA. Therapeutic approaches for long QT syndrome type 3: an update. *Europace* 2018;**20**:222–4.
- Dusi V, Pugliese L, De Ferrari GM, Odero A, Crotti L, Dagradi F *et al*. Left cardiac sympathetic denervation for long QT syndrome: 50 years' experience provides guidance for management. *JACC Clin Electrophysiol* 2022;**8**:281–94.
- Schwartz PJ, Spazzolini C, Priori SG, Crotti L, Vicentini A, Landolina M *et al*. Who are the long-QT syndrome patients who receive an implantable cardioverter-defibrillator and what happens to them?: data from the European long-QT syndrome implantable cardioverter-defibrillator (LQTS ICD) registry. *Circulation* 2010;**122**:1272–82.
- Martinez K, Bains S, Giudicessi JR, Bos JM, Neves R, Ackerman MJ. Spectrum and prevalence of side effects and complications with guideline-directed therapies for congenital long QT syndrome. *Heart Rhythm* 2022;**19**:1666–72.
- Moss AJ, Zareba W, Hall WJ, Schwartz PJ, Crampton RS, Benhorin J *et al*. Effectiveness and limitations of beta-blocker therapy in congenital long-QT syndrome. *Circulation* 2000;**101**:616–23.
- Gnecchi M, Stefanello M, Mura M. Induced pluripotent stem cell technology: toward the future of cardiac arrhythmias. *Int J Cardiol* 2017;**237**:49–52.
- Sala L, Gnecchi M, Schwartz PJ. Long QT syndrome modelling with cardiomyocytes derived from human-induced pluripotent stem cells. *Arrhythm Electrophysiol Rev* 2019;**8**:105–10.
- Gnecchi M, Sala L, Schwartz PJ. Precision medicine and cardiac channelopathies: when dreams meet reality. *Eur Heart J* 2021;**42**:1661–75.
- Castiglione A, Hornyik T, Wülfers EM, Giammarino L, Edler I, Jowais JJ *et al*. Docosahexaenoic acid normalizes QT interval in long QT type 2 transgenic rabbit models in a genotype-specific fashion. *Europace* 2022;**24**:511–22.
- Odening KE, Gomez A-M, Dobrev D, Fabritz L, Heinzel FR, Mangoni ME *et al*. ESC working group on cardiac cellular electrophysiology position paper: relevance, opportunities, and limitations of experimental models for cardiac electrophysiology research. *Europace* 2021;**23**:1795–814.
- ter Bekke RMA, Volders PGA. Arrhythmogenic mechano-electric heterogeneity in the long-QT syndrome. *Prog Biophys Mol Biol* 2012;**110**:347–58.
- Mazzanti A, Maragna R, Faragli A, Monteforte N, Bloise R, Memmi M *et al*. Gene-specific therapy with mexiletine reduces arrhythmic events in patients with long QT syndrome type 3. *J Am Coll Cardiol* 2016;**67**:1053–8.
- Das S, Aiba T, Rosenberg M, Hessler K, Xiao C, Quintero PA *et al*. Pathological role of serum- and glucocorticoid-regulated kinase 1 in adverse ventricular remodeling. *Circulation* 2012;**126**:2208–19.
- Bezzeresides VJ, Zhang A, Xiao L, Simonson B, Khedkar SA, Baba S *et al*. Inhibition of serum and glucocorticoid regulated kinase-1 as novel therapy for cardiac arrhythmia disorders. *Sci Rep* 2017;**7**:346.
- Itzhaki I, Maizels L, Huber I, Zwi-Dantsis L, Caspi O, Winterstern A *et al*. Modelling the long QT syndrome with induced pluripotent stem cells. *Nature* 2011;**471**:225–9.
- Bos JM, Crotti L, Rohatgi RK, Castelletti S, Dagradi F, Schwartz PJ *et al*. Mexiletine shortens the QT interval in patients with potassium channel-mediated type 2 long QT syndrome. *Circ Arrhythm Electrophysiol* 2019;**12**:e007280.
- Hwang J, Kim TY, Terentyev D, Zhong M, Kabakov AY, Bronk P *et al*. Late  $I_{Na}$  blocker GS967 suppresses polymorphic ventricular tachycardia in a transgenic rabbit model of long QT type 2. *Circ Arrhythm Electrophysiol* 2020;**13**:e006875.
- Imai S, Okayama N, Shimizu M, Itoh M. Increased intracellular calcium activates serum and glucocorticoid-inducible kinase 1 (SGK1) through a calmodulin-calcium calmodulin dependent kinase pathway in Chinese hamster ovary cells. *Life Sci* 2003;**72**:2199–209.
- Schwartz PJ, Crotti L, Insolia R. Long-QT syndrome: from genetics to management. *Circ Arrhythm Electrophysiol* 2012;**5**:868–77.
- Mura M, Pisano F, Stefanello M, Ginevrino M, Boni M, Calabrò F *et al*. Generation of two human induced pluripotent stem cell (hiPSC) lines from a long QT syndrome South African founder population. *Stem Cell Res* 2019;**39**:101510.

24. Ronchi C, Bernardi J, Mura M, Stefanello M, Badone B, Rocchetti M et al. NOS1AP polymorphisms reduce NOS1 activity and interact with prolonged repolarization in arrhythmogenesis. *Cardiovasc Res* 2021;**117**:472–83.
25. Mura M, Lee Y-K, Pisano F, Ginevrino M, Boni M, Calabrò F et al. Generation of the human induced pluripotent stem cell (hiPSC) line PSM1004-A from a carrier of the KCNQ1-R594Q mutation. *Stem Cell Res* 2019;**37**:101431.
26. Kagan A, Yu Z, Fishman GI, McDonald TV. The dominant negative LQT2 mutation A561V reduces wild-type HERG expression \*. *J Biol Chem* 2000;**275**:11241–8.
27. Mehta A, Sequiera GL, Ramachandra CJA, Sudibyo Y, Chung Y, Sheng J et al. Re-trafficking of hERG reverses long QT syndrome 2 phenotype in human iPSC-derived cardiomyocytes. *Cardiovasc Res* 2014;**102**:497–506.
28. Li G, Shi R, Wu J, Han W, Zhang A, Cheng G et al. Association of the hERG mutation with long-QT syndrome type 2, syncope and epilepsy. *Mol Med Rep* 2016;**13**:2467–75.
29. Crotti L, Lewandowska MA, Schwartz PJ, Insolia R, Pedrazzini M, Bussani E et al. A KCNH2 branch point mutation causing aberrant splicing contributes to an explanation of genotype-negative long QT syndrome. *Heart Rhythm* 2009;**6**:212–8.
30. Mura M, Mehta A, Ramachandra CJ, Zappatore R, Pisano F, Ciuffreda MC et al. The KCNH2-IVS9-28A/G mutation causes aberrant isoform expression and hERG trafficking defect in cardiomyocytes derived from patients affected by long QT syndrome type 2. *Int J Cardiol* 2017;**240**:367–71.
31. Nakajima T, Furukawa T, Tanaka T, Katayama Y, Nagai R, Nakamura Y et al. Novel mechanism of HERG current suppression in LQT2: shift in voltage dependence of HERG inactivation. *Circ Res* 1998;**83**:415–22.
32. Wang Z, Tristani-Firouzi M, Xu Q, Lin M, Keating MT, Sanguinetti MC. Functional effects of mutations in KvLQT1 that cause long QT syndrome. *J Cardiovasc Electrophysiol* 1999;**10**:817–26.
33. Brink PA, Crotti L, Corfield V, Goosen A, Durrheim G, Hedley P et al. Phenotypic variability and unusual clinical severity of congenital long-QT syndrome in a founder population. *Circulation* 2005;**112**:2602–10.
34. Heijman J, Spätiens RLHMG, Seyen SRM, Lentink V, Kuijpers HJH, Boulet IR et al. Dominant-negative control of cAMP-dependent IKs upregulation in human long-QT syndrome type 1. *Circ Res* 2012;**110**:211–9.
35. Huang L, Bitner-Glindzic M, Tranebjaerg L, Tinker A. A spectrum of functional effects for disease causing mutations in the Jervell and Lange-Nielsen syndrome. *Cardiovasc Res* 2001;**51**:670–80.
36. Kanki H, Kupersmidt S, Yang T, Wells S, Roden DM. A structural requirement for processing the cardiac K<sup>+</sup> channel KCNQ1. *J Biol Chem* 2004;**279**:33976–83.
37. Westenskow P, Splawski I, Timothy KW, Keating MT, Sanguinetti MC. Compound mutations: a common cause of severe long-QT syndrome. *Circulation* 2004;**109**:1834–41.
38. Wilson AJ, Quinn KV, Graves FM, Bitner-Glindzic M, Tinker A. Abnormal KCNQ1 trafficking influences disease pathogenesis in hereditary long QT syndromes (LQT1). *Cardiovasc Res* 2005;**67**:476–86.
39. Chouabe C, Neyroud N, Guicheney P, Lazdunski M, Romey G, Barhanin J. Properties of KvLQT1 K<sup>+</sup> channel mutations in Romano-Ward and Jervell and Lange-Nielsen inherited cardiac arrhythmias. *EMBO J* 1997;**16**:5472–9.
40. Ficker E, Dennis AT, Obejero-Paz CA, Castaldo P, Taglialatela M, Brown AM. Retention in the endoplasmic reticulum as a mechanism of dominant-negative current suppression in human long QT syndrome. *J Mol Cell Cardiol* 2000;**32**:2327–37.
41. Anderson CL, Delisle BP, Anson BD, Kilby JA, Will ML, Tester DJ et al. Most LQT2 mutations reduce Kv11.1 (hERG) current by a class 2 (trafficking-deficient) mechanism. *Circulation* 2006;**113**:365–73.
42. Mehta A, Ramachandra CJA, Singh P, Chitre A, Lua CH, Mura M et al. Identification of a targeted and testable antiarrhythmic therapy for long-QT syndrome type 2 using a patient-specific cellular model. *Eur Heart J* 2018;**39**:1446–55.
43. Tanaka T, Nagai R, Tomoike H, Takata S, Yano K, Yabuta K et al. Four novel KvLQT1 and four novel HERG mutations in familial long-QT syndrome. *Circulation* 1997;**95**:565–7.
44. Roden DM, Balsler JR. A plethora of mechanisms in the HERG-related long QT syndrome. Genetics meets electrophysiology. *Cardiovasc Res* 1999;**44**:242–6.
45. Sanguinetti MC, Curran ME, Spector PS, Keating MT. Spectrum of HERG K<sup>+</sup>-channel dysfunction in an inherited cardiac arrhythmia. *Proc Natl Acad Sci U S A* 1996;**93**:2208–12.
46. Lian X, Hsiao C, Wilson G, Zhu K, Hazeltine LB, Azarin SM et al. Robust cardiomyocyte differentiation from human pluripotent stem cells via temporal modulation of canonical Wnt signaling. *Proc Natl Acad Sci U S A* 2012;**109**:E1848–57.
47. Tohyama S, Hattori F, Sano M, Hishiki T, Nagahata Y, Matsuura T et al. Distinct metabolic flow enables large-scale purification of mouse and human pluripotent stem cell-derived cardiomyocytes. *Cell Stem Cell* 2013;**12**:127–37.
48. Buikema JW, Lee S, Goodyer WR, Maas RG, Chirikian O, Li G et al. Wnt activation and reduced cell-cell contact synergistically induce massive expansion of functional human iPSC-derived cardiomyocytes. *Cell Stem Cell* 2020;**27**:50–63.e5.
49. Sala L, Leonov V, Mura M, Giannetti F, Khudiakov A, Moretti A et al. Use of hiPSC-derived cardiomyocytes to rule out proarrhythmic effects of drugs: the case of hydroxychloroquine in COVID-19. *Front Physiol* 2022;**12**:730127.
50. Burridge PW, Matsa E, Shukla P, Lin ZC, Churko JM, Ebert AD et al. Chemically defined generation of human cardiomyocytes. *Nat Methods* 2014;**11**:855–60.
51. Shaheen N, Shiti A, Huber I, Shinnawi R, Arbel G, Gepstein A et al. Human induced pluripotent stem cell-derived cardiac cell sheets expressing genetically encoded voltage indicator for pharmacological and arrhythmia studies. *Stem Cell Reports* 2018;**10**:1879–94.
52. Bazett HC. An analysis of the time-relations of electrocardiograms. *Ann Noninvasive Electrocardiol* 1997;**2**:177–94.
53. Brunner M, Peng X, Liu GX, Ren X-Q, Ziv O, Choi B-R et al. Mechanisms of cardiac arrhythmias and sudden death in transgenic rabbits with long QT syndrome. *J Clin Invest* 2008;**118**:2246–59.
54. Odening KE, Bodi I, Franke G, Rieke R, Ryan de Medeiros A, Perez-Feliz S et al. Transgenic short-QT syndrome 1 rabbits mimic the human disease phenotype with QT/action potential duration shortening in the atria and ventricles and increased ventricular tachycardia/ventricular fibrillation inducibility. *Eur Heart J* 2019;**40**:842–53.
55. Barry PH, Lynch JW. Liquid junction potentials and small cell effects in patch-clamp analysis. *J Membr Biol* 1991;**121**:101–17.
56. Shinnawi R, Shaheen N, Huber I, Shiti A, Arbel G, Gepstein A et al. Modeling reentry in the short QT syndrome with human-induced pluripotent stem cell-derived cardiac cell sheets. *J Am Coll Cardiol* 2019;**73**:2310–24.
57. Verheijck EE. Perforated patch-clamp technique in heart cells. In: Van Duijn B, Wiltink A (eds). *Signal transduction—single cell techniques*. Berlin, Heidelberg: Springer Berlin Heidelberg; 1998:207–13.
58. Terentyev D, Rees CM, Li W, Cooper LL, Jindal HK, Peng X et al. Hyperphosphorylation of RyRs underlies triggered activity in transgenic rabbit model of LQT2 syndrome. *Circ Res* 2014;**115**:919–28.
59. Shimizu W, Antzelevitch C. Sodium channel block with mexiletine is effective in reducing dispersion of repolarization and preventing torsades des pointes in LQT2 and LQT3 models of the long-QT syndrome. *Circulation* 1997;**96**:2038–47.
60. Aoyama T, Matsui T, Novikov M, Park J, Hemmings B, Rosenzweig A. Serum and glucocorticoid-responsive kinase-1 regulates cardiomyocyte survival and hypertrophic response. *Circulation* 2005;**111**:1652–9.
61. Kim M, Sager PT, Tester DJ, Pradhananga S, Hamrick SK, Srinivasan D et al. SGK1 inhibition attenuates the action potential duration in re-engineered heart cell models of drug-induced QT prolongation. *Heart Rhythm* 2023;**20**:589–95.
62. Yang T, Chun YW, Stroud DM, Mosley JD, Knollmann BC, Hong C et al. Screening for acute IKr block is insufficient to detect torsades de pointes liability: role of late sodium current. *Circulation* 2014;**130**:224–34.
63. Morgat C, Denjoy I, Fressart V, Badilini F, Vaglio M, Messali A et al. ECG descriptors of ventricular repolarization are associated with cardiac events in a gene-specific manner in long QT syndrome patients. *Europace* 2022;**24**:eua053.555.
64. Bárándi L, Virág L, Jost N, Horváth Z, Koncz I, Papp R et al. Reverse rate-dependent changes are determined by baseline action potential duration in mammalian and human ventricular preparations. *Basic Res Cardiol* 2010;**105**:315–23.
65. Varró A, Baczkó I. Cardiac ventricular repolarization reserve: a principle for understanding drug-related proarrhythmic risk. *Br J Pharmacol* 2011;**164**:14–36.
66. Seeböhm G, Strutz-Seeböhm N, Ureche ON, Henrion U, Baltaev R, Mack AF et al. Long QT syndrome-associated mutations in KCNQ1 and KCNE1 subunits disrupt normal endosomal recycling of IKs channels. *Circ Res* 2008;**103**:1451–7.
67. Kim M, Das S, Tester DJ, Pradhananga S, Hamrick SK, Gao X et al. SGK1 inhibition attenuated the action potential duration in patient- and genotype-specific re-engineered heart cells with congenital long QT syndrome. *Heart Rhythm* 2023. <https://doi.org/10.1016/j.hrro.2023.02.003>
68. Wilde AAM, Semsarian C, Márquez MF, Shamloo AS, Ackerman MJ, Ashley EA et al. European Heart Rhythm Association (EHRA)/Heart Rhythm Society (HRS)/Asia Pacific Heart Rhythm Society (APHRS)/Latin American Heart Rhythm Society (LAHRS) Expert Consensus Statement on the state of genetic testing for cardiac diseases. *Europace* 2022;**24**:1307–67.
69. Schwartz PJ, Priori SG, Spazzolini C, Moss AJ, Vincent GM, Napolitano C et al. Genotype-phenotype correlation in the long-QT syndrome: gene-specific triggers for life-threatening arrhythmias. *Circulation* 2001;**103**:89–95.